Cite this: DOI: 10.1039/c0xx00000x

www.rsc.org/xxxxxx

ARTICLE TYPE

Using multi-walled carbon nanotubes to enhance coimmobilization of poly(azure A) and poly(neutral red) for determination of nicotinamide adenine dinucleotide and hydrogen peroxide

Kuo Chiang Lin, A.T. Ezhil Vilian and Shen Ming Chen*

Received (in XXX, XXX) Xth XXXXXXXXX 20XX, Accepted Xth XXXXXXXXX 20XX
DOI: 10.1039/b000000x

Coimmobilization of poly(azure A) (PAA) and poly(neutral red) (PNR) has been successfully performed and further enhanced by a multi-walled carbon nanotubes (MWCNTs) modified electrode. The PAA-PNR/MWCNTs hybrid composite is electroactive, pH-dependent, and stable in the electrochemical system. It shows eletrocatalytic activity to nicotinamide adenine dinucleotide (NADH) and hydrogen peroxide (H_2O_2) with high current response and low overpotential. By amperometry, it shows a high sensitivity of 265.8 μA mM^{-1} cm^{-2} to NADH ($E_{app.}$ = +0.05 V). Linearity is estimated in a concentration range of 1×10^{-6}–1.455×10^{-3} M with a detection limit of 1×10^{-7} M (S/N = 3). It shows a high sensitivity of 10.3 μA mM^{-1} cm^{-2} to H_2O_2 ($E_{app.}$ = -0.25 V) with a linear concentration range of 8×10^{-4}–1.91×10^{-3} M and a detection limit of 1×10^{-6} M (S/N = 3). By the result, it proves the coimmobilization and activity of PAA and PNR can be effectively enhanced by MWCNTs, suggesting a bifunctional sensor for determination of NADH and H_2O_2.

1. Introduction

Reduced NADH and its oxidized form, NAD^+, are very important coenzymes that play an important role in the energy production/consumption of cells of all living organisms. NADH participates in a variety of enzymatic reactions via more than 300 dehydrogenases.[1] Thus, many studies have focused on the fundamental scientific applications of the NADH reaction. It has received considerable interest due to its very important role as a cofactor in a whole diversity of dehydrogenase-based bioelectrochemical devices such as biosensors, biofuel cells, and bioreactors.[2–4] However, direct oxidation of NADH at a conventional solid electrode is highly irreversible, requires large activation energy, and proceeds with coupled side reactions, poisoning the electrode surface.[5–7] In recent years, many nanomaterials, especially various carbon nanomaterials,[8–10] have been used widely to reduce the over-potential for NADH oxidation and minimize the surface contamination effect without the help of redox mediators.

The rapid and accurate determination of H_2O_2 is of great importance in pharmaceutical, clinical, industrial, and environmental analyses. Many techniques have been employed for the determination of H_2O_2, such as titrimetry, photometry, chemiluminescence, high performance liquid chromatography and electrochemistry.[11] Among these techniques, amperometric enzyme-based biosensors have received considerable attention due to its convenience, high sensitivity and selectivity.[12] In order to prepare excellent biosensors, many materials were employed to improve the microenvironment around proteins, provide suitable orientation, and accelerate the electron transfer between protein and the electrode surface.[13] Generally, the electrodes were modified with biomolecules films,[14] conducting polymers,[15] redox dyes[16] and nanoparticles.[17] Conducting polymers and nanomaterials[18–20] have attracted great research interest in biosensor due to their versatility of the physical and chemical properties. In our studies, we ever used azine redox dyes to immobilize flavin adenine dinucleotide on the electrode surface and it has been noticed to reduce H_2O_2 due to its good electrocatalytic reduction property.[21,22] It indicates that the conducting polymers can be arranged as hybrid composites with active species and their electrocatalytic properties can be further enhanced. However, one might suffer the difficulty of polymer chains disorder during the hybrid film formation. It is worthy to study the hybrid film formation and consider the enhancement of their electrocatalytic properties.

For two decades carbon nanotubes (CNTs) have been gaining popularity due to their unique properties such as electronic, metallic and structural characteristics.[23] CNTs have outstanding ability to mediate fast electron transfer kinetics for a wide range of electroactive species and show electrocatalytic activity towards biologically important compounds such as NADH[24] and H_2O_2.[25] Recently, the fabrication of CNTs/conducting polymer composites has gained great interest as the CNTs can improve the electrical and mechanical properties of polymers[26,27] and it has been demonstrated that the obtained CNTs/conducting polymer possess properties of the individual components with a synergistic effect.[28–33] Particularly, CNTs might play a role as a template to immobilize conducting polymers especially for different conducting polymers coimmobilization.

In the present investigation, azure A (AA) a phenothiazine redox dye and neutral red (NR) a phenazine redox dye are proposed to co-immobilize on electrode surface because they have an amino group located on the heteroaromatic azine ring, makes them amenable to facilitate electropolymerization,[34] and their good activities also have been gradually disclosed in the literature.[22,35–37] The use of CNTs to improve the coimmobilization of conducting polymers and the electrocatalytic property is also studied.

In this work, a simple electrochemical synthesis of PAA and PNR hybrid composites using MWCNTs-electrode is studied. This hybrid composite can be easily prepared on electrode surface through electropolymerization of AA and NR monomers under suitable potential control. The hybrid composites are electrochemically characterized and the electrocatalytic reactions of NADH and H_2O_2 are also investigated.

2. Experimental

2.1 Materials and apparatus

NADH, H_2O_2, azure A, neutral red, and MWCNTs were purchased from Sigma-Aldrich (USA) and were used as received. All other chemicals (Merck) used were of analytical grade (99%). Double-distilled deionized water (> 18.1 MΩ cm^{-1}) was used to prepare all the solutions. All other reagents were of analytical grade and used without further purification.

The hybrid composite of PAA-PNR/MWCNTs was characterized by cyclic voltammetry, electrochemical impedance spectroscopy, and amperometry. A glassy carbon electrode (GCE) was purchased from Bioanalytical Systems (BAS) Inc., USA. All GCEs were used with diameter of ϕ = 0.3 cm (exposed geometric surface area of A = 0.0707 cm^2) for all electrochemical techniques except of amperometry (ϕ = 0.6 cm; A = 0.2826 cm^2) because of the difference between CV equipment and amperometry equipment. The sensitivity is calculated in the unit of [(current response)/(analyte concentration*electrode surface area)] so that no influence in the comparison. Electrochemical experiments were completed by a CHI 1205a electrochemical workstation (CH Instruments, USA) with a conventional three-electrode setup containing a GCE, an Ag/AgCl (3 M KCl) electrode, and a platinum wire as working, reference, and counter electrode, respectively. The morphological characterization of composite films was examined by means of SEM (S-3000H, Hitachi). All electrochemical impedance spectroscopy (EIS) experiments were examined in pH 7 PBS containing 5×10^{-3} M $Fe(CN)_6^{3-/4-}$. The applied potential was 5 mV and the frequency range was analyzed in the range from 0.1 MHz to 0.1 Hz. The buffer solution was entirely deaerated using nitrogen gas atmosphere.

2.2 Fabrication of PAA-PNR and PAA-PNR/MWCNTs modified electrodes

The MWCNTs modified electrode was prepared with well-dispersed MWCNTs suspension. The MWCNTs were dissolved in N,N-dimethylformamide (1 mg ml^{-1}) with sonication for 30 minutes. By drop casting method, 10 μl of the suspension was dropped on electrode surface and dried out in the oven at 40 ℃. Consequently, it was transferred to have hybrid electropolymerization of AA and NR in pH 7 phosphate buffer solution (PBS) containing 2.5×10^{-5} M AA and 2.5×10^{-4} M NR by consecutive cyclic voltammetry. Potential cycling was controlled in the potential range of -0.8 ~ +0.8 V and scan rate of 0.1 Vs^{-1} with 20 scan cycles. After this procedure, the PAA-PNR and PAA-PNR/MWCNTs modified electrodes were prepared to study.

3. Results and discussion

3.1 Preparation and characterization of PAA-PNR/MWCNTs

3.1.1 Preparation of PAA-PNR/MWCNTs hybrid composite

PAA and PNR are used to modify electrode surface because both of them are active for NADH oxidation. The coimmobilization of PAA and PNR is arranged and expected for advanced activity in this work. According to previous works,[22,34–37] PAA and PNR can be individually prepared on an electrode surface involving electropolymerization of AA and NR monomers. This is the first time to immobilize both PAA and PNR on electrode surface.

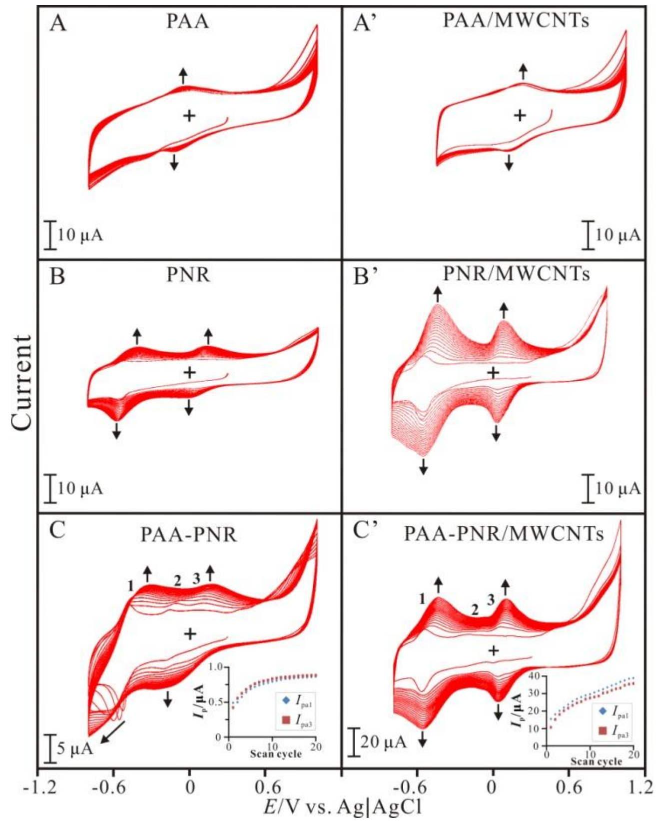

Fig. 1. Consecutive cyclic voltammograms of PAA, PNR, PAA-PNR examined in pH 7 PBS containing 2.5×10^{-4} M AA with/without 2.5×10^{-4} M NR using GCE (A — C) and MWCNTs/GCE (A'—C'). Scan rate = 0.1 Vs^{-1}. Insets of (C) and (C'): the plots of peak current (I_{pa1}, I_{pa3}) vs. scan cycle.

Fig. 1 shows the voltammograms for the electropolymerization of AA and NR using bare GCE and MWCNTs/GCE, respectively. All experiments were taken in the potential range of -0.8—1.0 V with 20 scan cycles and scan rate of 0.1 Vs^{-1}. Fig. 1A and 1A' depict the voltammograms of AA electropolymerization using a GCE and MWCNTs/GCE. It shows a redox couple with increase in the redox peak currents. The electropolymerization of assembled AA was performed in pH 7 PBS by cyclic voltammetry. Fig. 1A and 1A' is the typical set of cyclic voltammogram obtained from the electropolymerization of AA assembled on the GCE and MWCNTs/GCE, respectively. The cyclic voltammograms show that the cathodic current of AA monomer decreased at about -0.25V while the cathodic current of PAA increased at about -0.06 V, which means both of the assembled AA could be electropolymerized to form conducting polymer successfully. The two cyclic voltammograms are very similar, indicating that the structure of PAA didn't change on the surface of MWCNTs. Current response is the only difference between two electropolymerization procedures using GCE and MWCNTs/GCE. The above results have a good agreement with the previous work.[35]

Fig. 1B and 1B' depict the voltammograms of NR electropolymerization using a GCE and MWCNTs/GCE. It shows two redox couples with increase in the redox peak currents. The electropolymerization of assembled NR was performed in pH 7 PBS by cyclic voltammetry. Fig. 1B and 1B' is the typical set of cyclic voltammogram obtained from the electropolymerization of NR assembled on the GCE and MWCNTs/GCE, respectively. Considering the electrochemical process, there are one anodic peak at -0.54 V and one cathodic peak at -0.59 V for the first cycle. The anodic peak at 0.7 V corresponds to the formation of the radical cation dye. The anodic peak current at about 0.02 V and the corresponding cathodic peak current at 0.08 V increase with the number of potential cycles, indicating a successive increase in the amount of the poly(neutral red) film. Therefore, two redox couples are found at the formal potential of $E_1^{0'}$ = -0.56 V and $E_3^{0'}$ = +0.05 V in the cyclic voltammogram of PNR formation. Similarly, two significant redox couples are found at the formal potential of $E_1^{0'}$ = -0.54 V and $E_3^{0'}$ = +0.05 V in the case using MWCNTs/GCE. It means the same electrochemical processes of NR electropolymerization occur using both bare GCE and MWCNTs/GCE. Moreover, the higher current response is found in the case using MWCNTs/GCE. It indicates that higher current response of NR electropolymerization can be enhanced by MWCNTs. The corresponding results have a good agreement with the previous works.[22,37]

As shown in Fig. 1C, the coimmobilization of PAA and PNR were carried out in pH 7 PBS containing 2.5×10^{-5} M AA and 2.5×10^{-4} M NR by consecutive cyclic voltammetry. The cyclic voltammogram depicts the electropolymerization of AA and NR on bare electrode surface. All peak currents are increasing as the increase in the scan cycles. It exhibits three redox couples at the formal potential of $E_1^{0'}$ = -0.58 V, $E_2^{0'}$ = -0.18 V, and $E_3^{0'}$ = +0.02 V. However, the redox peaks enormously shift especially the cathodic peak 1. This phenomenon might be caused by the disorder of hybrid films formation. In order to overcome this drawback, a strategy is proposed to enhance the electropolymerization of PAA and PNR hybrid films using MWCNTs as an active and steric template. Fig. 1C' shows the voltammogram of AA and NR electropolymerization using a MWCNTs-electrode in the same solution. It exhibits significant redox couples at the formal potential of $E_1^{0'}$ = -0.53 V, $E_2^{0'}$ = -0.15 V, and $E_3^{0'}$ = +0.05 V, corresponding to the related redox couples of AA and NR electropolymerization. The corresponding results have a good agreement with the previous works.[22,35,37] Furthermore, one can see that three redox couples have well current development with less peak shift as the increase in scan cycles. It can be concluded that the hybrid films formation can be improved by MWCNTs. Insets of Fig. 1C and 1C' present the peak currents (I_{pa1} and I_{pa3}) development with scan cycles. Both bare and modified electrodes have current increase at the redox peaks. During 20 scan cycles, the MWCNTs-electrode shows higher current response and sharp increasing curve different from bare electrode (Insets of Fig. 1C and 1C'). It indicates that MWCNTs provides more active space allowed PAA and PNR coimmobilize on electrode surface result in well redox peaks with high peak current and less peak shift. One can know that the hybrid films formation of PAA and PNR can be improved by MWCNTs.

3.1.2 Characterization of PAA-PNR/MWCNTs hybrid composite by SEM, cyclic voltammetry, and EIS

Surface morphology of these modified electrodes was studied by SEM. Fig. 2 shows the SEM images for (A) bare, (B) PAA, (C) PNR, (D) PAA-PNR, (A') MWCNTs, (B') PAA/MWCNTs, (C') PNR/MWCNTs, and (D') PAA-PNR/MWCNTs coated ITO electrodes.

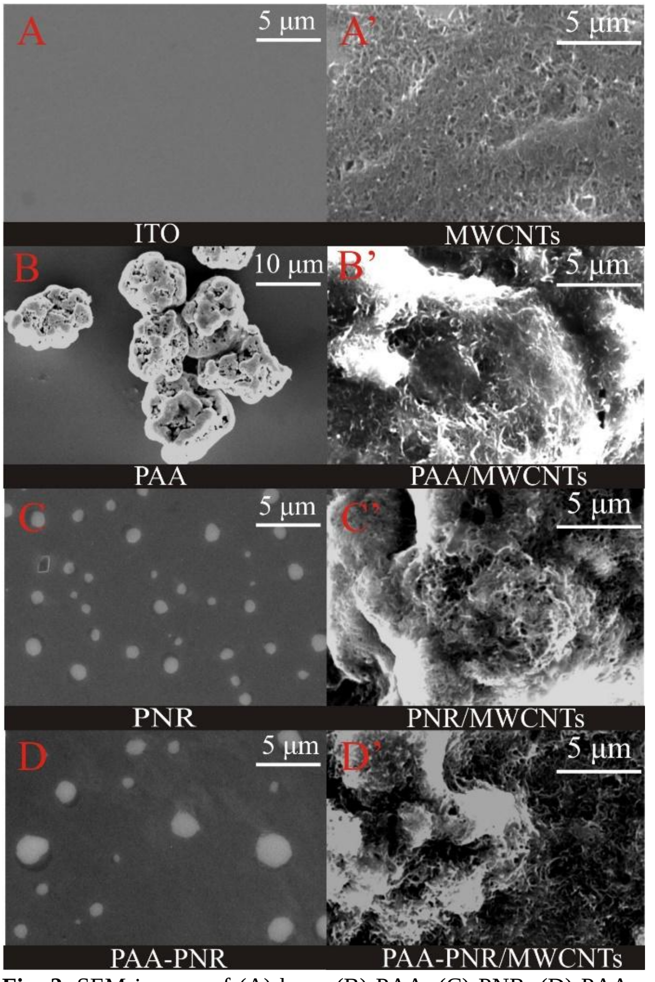

Fig. 2. SEM images of (A) bare, (B) PAA, (C) PNR, (D) PAA-PNR, (A') MWCNTs, (B') PAA/MWCNTs, (C') PNR/MWCNTs, and (D') PAA-PNR/MWCNTs coated ITO electrodes.

Fig. 2A−2D and 2A'−2D' represent the images for various modified electrodes "without" and "with" MWCNTs. PAA, PNR and PAA-PNR (Fig. 2B−2D) exhibit globular structures due to the clusters formation in the electropolymerization process. Particularly, PAA has bigger clusters among these materials. Considering the AA electropolymerization, the voltammograms (Fig. 1A and 1A') show less increase in the redox peak currents. It indicates the bigger PAA clusters formation might be easier cause the termination of AA electropolymerization. Therefore, it shows less increase in redox peak currents and big clusters in SEM images.

It exhibits the fiber-like structure when MWCNTs coated on electrode surface (Fig. 2A'). Fig. 2B' − 2D' show the SEM images for PAA/MWCNTs, PNR/MWCNTs, and PAA-PNR/MWCNTs, respectively. They show globular clusters and fiber-like structure. By comparison, it exhibits more compact morphological image when using a MWCNTs-electrode to do the electropolymerization of AA, NR, and both of them. One can conclude that MWCNTs can enhance the immobilization of PAA, PNR, and both of them.

To ascertain the hybrid composite successfully immobilized on electrode surface, the PAA-PNR/MWCNTs modified electrode was examined in pH 7 PBS and compared to the relative modified electrodes. Fig. 3 shows the voltammograms of (a) PAA, (b) PNR, (c) PAA-PNR, and (d) PAA-PNR/MWCNTs modified electrodes examined in pH 7 PBS. The PAA-PNR/MWCNTs composite shows obvious three redox couples with smaller peak-to-peak separation and higher current response. By comparison, the current response of PAA-PNR/MWCNTs is several folds of other modifiers. By the comparison of CV and SEM results, it indicates that PAA-PNR-MWCNTs hybrid composite is more reversible, active and compact in the related modifiers.

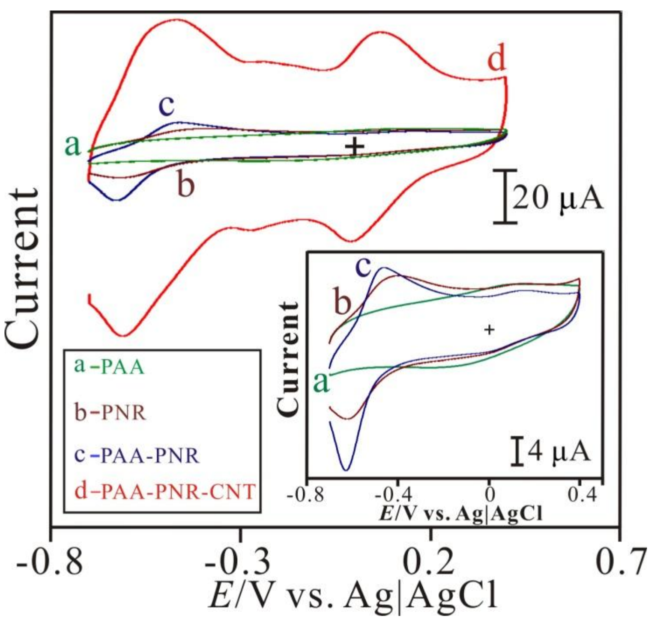

Fig. 3. Cyclic voltammograms of (a) PAA, (b) PNR, (c) PAA-PNR, and (d) PAA-PNR/MWCNTs modified electrodes examined in pH 7 PBS. Scan rate = 0.1 Vs^{-1}. Inset: the scale-up voltammograms of (a) PAA, (b) PNR, and (c) PAA-PNR.

The PAA-PNR/MWCNTs composite was further electrochemically characterized by EIS. EIS can give information on the impedance changes of the electrode surface during the modification process. EIS spectra usually provide the semicircle arc at higher frequencies correspond to the electron transfer limited process or the electron transfer resistance (R_{et}). One can easily determine R_{et} to understand the relationship between impedance and modifiers on the electrode interface. Fig. 4 shows the EIS spectra of (a) bare, (b) PAA/MWCNTs, (c) MWCNTs, (d) PNR/MWCNTs, and (e) PAA-PNR/MWCNTs modified electrode examined in pH 7 PBS containing 5×10^{-3} M $Fe(CN)_6^{3-/4-}$. Curve (a) shows the EIS spectra of the bare GCE which exhibits a straight line and a large semicircle arc (R_{et} = 798.2 Ω). Curve (b)-(e) individually depicts a straight line with a smaller depressed semicircle arc estimated in R_{et} = 119.2 Ω, 73.2 Ω, 71.2 Ω, and 48.2 Ω for (b) PAA/MWCNTs/GCE, (c) MWCNTs/GCE, (d) PNR/MWCNTs/GCE, and (e) PAA-PNR/MWCNTs/GCE, respectively. They present a resistance of electrolytic solution (R_s) about 90.8 Ω. One can know that the modified electrodes exhibit lower R_{et} than that of bare GCE. This phenomenon indicates that the electroactive species can lower the resistance of electron transfer and effectively enhance the activity on electrode surface. Particularly, the PAA-PNR/MWCNTs/GCE shows relatively lower resistance which is even lower than that of MWCNTs/GCE. It implies that the PAA and PNR are well immobilized on MWCNTs to form a compact and active hybrid composite result in low electron transfer resistance and high current response.

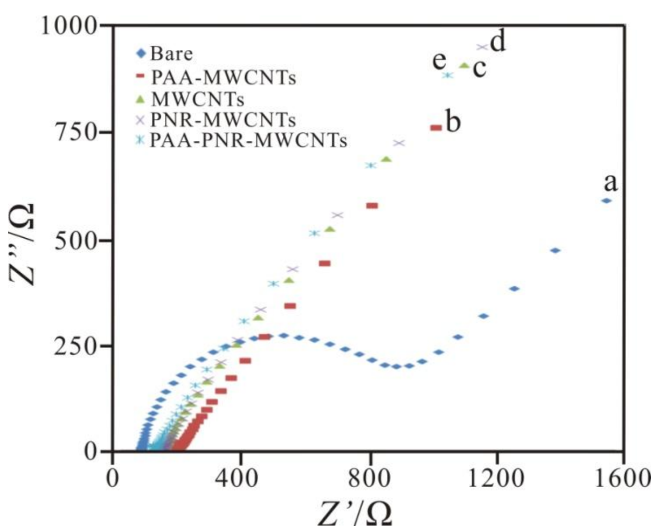

Fig. 4. EIS spectra of (a) bare, (b) PAA-MWCNTs, (c) MWCNTs, (d) PNR-MWCNTs, and (e) PAA-PNR/MWCNTs modified electrode examined in pH 7 PBS containing 5×10^{-3} M $Fe(CN)_6^{3-/4-}$.

The influence of the scan rate and pH condition on the PAA-PNR/MWCNTs/GCE electrochemical response was also studied. Fig. 5A shows the cyclic voltammograms of PAA-PNR/MWCNTs/GCE examined with different scan rate in pH 7 PBS. According to the obvious redox couples, it represents that the PAA-PNR/MWCNTs can be well immobilized on GCE and it can show stable current response in the scan rate of 10−1000 mVs^{-1}. In the potential range of -0.8 V to +0.4 V, the PAA-PNR/MWCNTs film exhibits three well-defined redox couples with smaller peak-to-peak separation, indicating reversible and fast electron transfer processes. Both anodic and cathodic peak currents are directly proportional to scan rate (inset of Fig. 5A), suggesting a surface controlled process in the electrochemical system. The observation of well-defined and persistent cyclic voltammetric peaks indicates that the PAA-PNR/MWCNTs/GCE exhibits electrochemical response characteristics of redox species confined on the electrode. The apparent surface coverage (Γ) was estimated by following equation:

$$I_p = n^2F^2 v A \Gamma / 4RT \quad (1)$$

where, I_p is the peak current of the PAA-PNR/MWCNTs composite electrode; n is the number of electron transfer; F is Faraday constant (96485 C mol^{-1}); v is the scan rate (mV s^{-1}); A is the area of the electrode surface (0.07 cm^2); R is gas constant (8.314 J mol^{-1} K^{-1}); and T is the room temperature (298.15 K). The anodic peak 1, 2, and 3 are used for the calculation of the apparent surface coverage of NR, PAA, and PNR. Assuming a two-electron process in the present case, the Γ was calculated in 9.2×10^{-10} mol cm^{-2}, 5.9×10^{-10} mol cm^{-2}, and 1.1×10^{-9} mol cm^{-2} for PAA, NR, and PNR, respectively.

These values are several folds of that in previous works of PAA, NR, and PNR.[35–37] High surface coverage indicates that the hybrid composite might be compact with more electroactive species on electrode surface. One can conclude that MWCNTs provides more active sites to load more electroactive species.

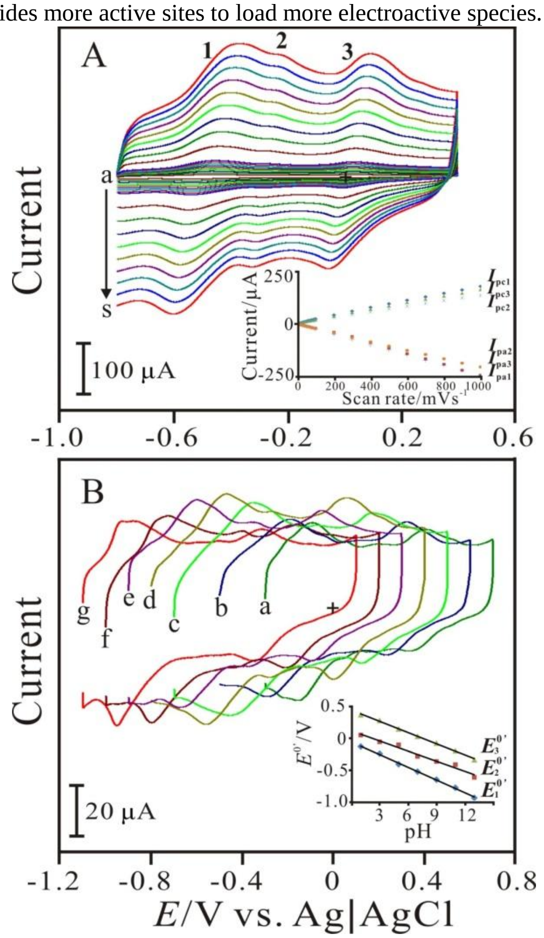

Fig. 5. Cyclic voltammograms of PAA-PNR/MWCNTs/GCE examined with (A) 10－1000 Vs^{-1} (pH 7 PBS) and (B) pH 1－13 (scan rate = 0.1 Vs^{-1}). Insets are plots of peak current vs. scan rate and formal potential ($E^{0'}$) vs. pH.

To ascertain the effect of pH, PAA-PNR/MWCNTs/GCE was examined in different pH solutions (pH 1 – 13). Fig. 5B presents the PAA-PNR/MWCNTs redox peaks which are shifted to more negative potential as increasing pH value of solution. It shows stable redox peaks in various pH conditions. This result is the same even though PAA-PNR/MWCNTs is repeatedly examined and change testing order of pH condition. It indicates that PAA-PNR/MWCNTs hybrid composite is active and stable in wide pH condition. The characteristic PNR redox couples (with formal potential of $E^{0'}_1$ and $E^{0'}_3$) exhibit the significant slopes of -65.9 mV pH^{-1} and -52.7 mV pH^{-1} for redox couple 1 and redox couple 3, respectively. The PAA redox couple ($E^{0'}_2$) is also pH-dependent with a slope of -58.1 mV pH^{-1} with the increase of pH value. These slopes are close to that given by the Nernstian equation, suggesting a two-electron and two-proton transfer for PAA, NR, and PNR redox processes. This phenomenon indicates that both PAA and PNR redox processes are involving two-proton and two-electron transfer processes in the electrochemical system. It represents the electrochemical behaviours through the reduction and oxidation states for PAA and PNR and the results are also close to previous reports.[22,36] As the result, the hybrid composites can be stable and electroactive in the different pH buffer solutions.

3.2 Electrocatalysis of NADH and H_2O_2 at PAA-PNR/MWCNTs electrode

The electrocatalytic activity of the PAA-PNR/MWCNTs electrode towards the oxidation of NADH and the reduction of H_2O_2 in pH 7 PBS was demonstrated.

Fig. 6A displays the CVs of PAA-PNR/MWCNTs/GCE in pH 7 PBS containing different concentration of NADH (a－d). PAA-PNR/MWCNTs/GCE shows an obvious oxidation peak at about +0.05 V with high peak current while bare GCE (a') shows an oxidation peak at +0.7 V for NADH. Fig. 6B displays the CVs of PAA-PNR/MWCNTs/GCE in pH 7 PBS containing different concentration of H_2O_2 (a－d). PAA-PNR/MWCNTs/GCE shows two obvious reduction peaks at about -0.25 V and -0.55 V with high peak current while bare GCE (a') shows almost no reduction peak in this potential range.

Table 1 shows the activity comparison of PAA-PNR/MWCNTs compared with related modifiers for electrocatalytic oxidation of NADH in pH 7 PBS. Most higher net current response is found in PAA-PNR/MWCNTs and it has competitive lower overpotential in these series of modifiers. By comparison, the sensitivity of PAA-PNR/MWCNTs electrode towards NADH is much higher than those of PAA and PNR. This result proves that the activity of PAA and PNR can be enhanced by MWCNTs. It also means that the hybrid composite can effectively alternate electrode interface result in good electrocatalytic activity towards both NADH oxidation and H_2O_2 reduction. It is concluded that PAA-PNR/MWCNTs is active with low overpotential and high current response, suggesting a bifunctional sensor for determination of NADH and H_2O_2.

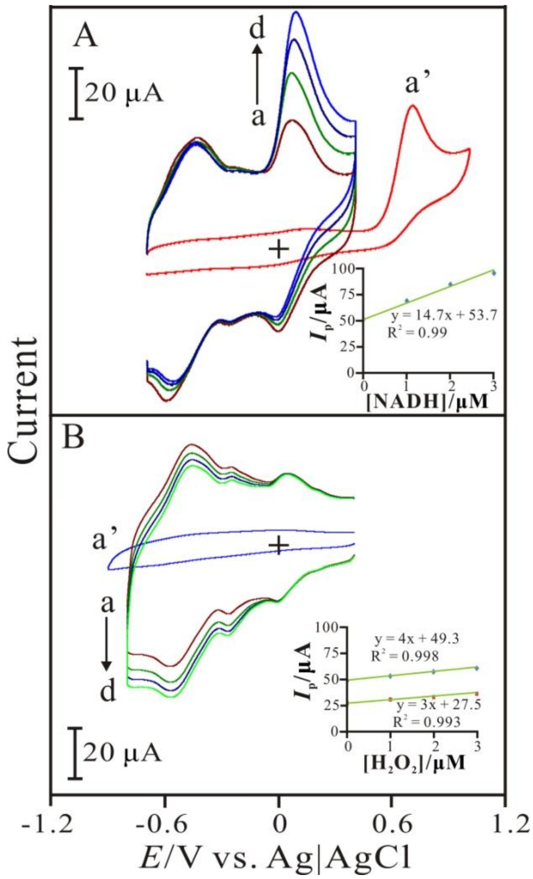

Fig. 6. Cyclic voltammograms of PAA-PNR/MWCNTs/GCE examined in pH 7 PBS containing (A) [NADH] = (a) 0 μM, (b) 1 μM, (c) 2 μM, and (d) 3 μM; (B) $[H_2O_2]$ = (a) 0 μM, (b) 1 μM, (c) 2 μM, and (d) 3 μM, respectively. Scan rate = 0.1 Vs^{-1}. (a') is voltammogram of bare electrode in the presence of target species. Insets: the plots of peak current vs. species concentration.

Table 1. Activity comparison of PAA-PNR/MWCNTs compared with related modifiers for electrocatalytic oxidation of NADH in pH 7 PBS.

Modifiers	$E_{obs.}$[a]/V	I_{pb}[b]/μA	I_{pa}[c]/μA	ΔI_{pa}[d]/ μA	Current Ratio[e]
PAA	0.28	6.4	7.1	0.7	1
PNR	0.13	6.2	6.7	0.5	0.7
PAA-PNR	0.20	5.9	6.2	0.3	0.4
MWCNTs	0.28	6.9	44.6	37.7	54
PAA/MWCNTs	0.04	13.7	24.5	10.8	15
PNR/MWCNTs	0.04	17.5	28	10.5	15
PAA-PNR/MWCNTs	0.05	52.3	96.6	44.3	63

[a] The anodic peak potentail observed for NADH oxidaiton.
[b] The anodic peak current measured in the absence of 3 μM NADH.
[c] The anodic peak current measured in the presence of 3 μM NADH.
[d] Net current contribution ($\Delta I_{pa} = I_{pa} - I_{pb}$) estimated from anodic peak current in the blank (I_{pb}) and anodic peak current in the presence of NADH (I_{pa}).
[e] Current ratio is estimated based on the net current contribution of PAA for NADH oxidaiton.

3.3 Amperometric response of PAA-PNR/MWCNTs composite to NADH and H_2O_2

Fig. 7A & B show amperometric responses of PAA-PNR/MWCNTs modified electrode with additions of NADH and H_2O_2 obtained by amperometry. They were carried out with electrode rotation speed of 1000 rpm and individually applied potential at +0.05 V and -0.25 V, respectively. PAA-PNR/MWCNTs/GCE shows significant amperometric response for NADH and H_2O_2 addition spiked by micro-syringe. Insets of Fig. 7 present the calibration curves, the regression equations are obtained as $I_{NADH}(\mu A) = 0.0751C_{NADH}(\mu M) + 4$ and $I_{H2O2}(\mu A) = 0.0029C_{H2O2}(\mu M) + 27.7$, with correlation coefficient of R^2 = 0.9947 and 0.9951, respectively. As the results, it provides linear concentration range of 1×10^{-6}–1.455×10^{-3} M with sensitivity of 265.8 μA mM^{-1} cm^{-2} and detection limit of 1×10^{-7} M (S/N = 3) for NADH. In the case of H_2O_2 reduction, it also provides linear concentration range of 8×10^{-4}–1.91×10^{-3} M with sensitivity of 10.3 μA mM^{-1} cm^{-2} and detection limit of 1×10^{-6} M (S/N = 3).

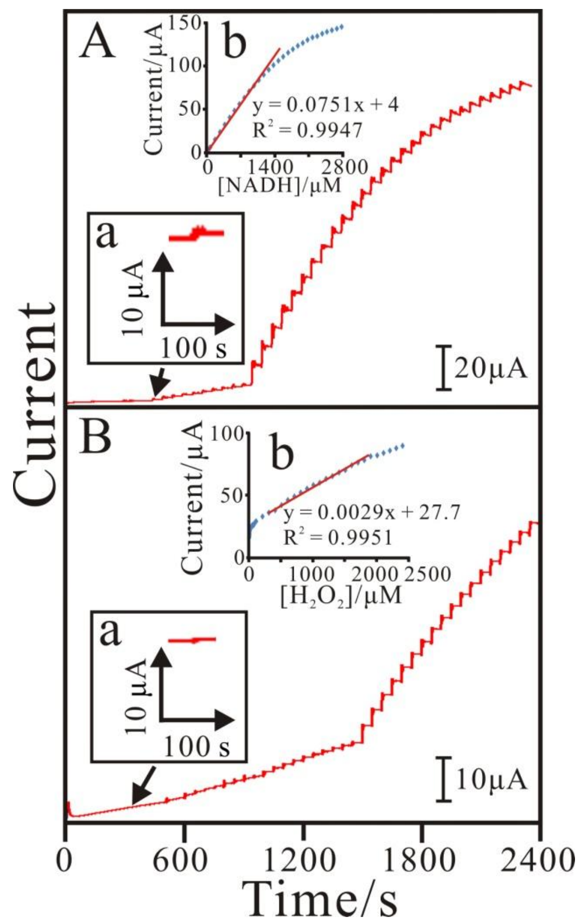

Fig. 7. Amperograms of PAA-PNR/MWCNTs/GCE examined with additions of (A) NADH ($E_{app.}$ = +0.05 V) and (B) H_2O_2 ($E_{app.}$ = -0.25 V). Electrode rotation speed = 1000 rpm. Insets: (a) the steady-state current–response time of PAA-PNR/MWCNTs/GCE to NADH and H_2O_2; (b) the calibration graph for NADH and H_2O_2.

Table 2 presents the main performances of published data about NADH sensors based on different modified materials. By comparison, the NADH sensor presented in this paper exhibits one of the highest sensitivity with a low detection limit and very low overpotential. A significant lower detection limit and a higher sensitivity were reported for sensors based on MWCNTs. They might prove that the synergistic effect of obtained CNTs/conducting polymer possess properties of the individual components similar to previous reports.[28–33] Table 3 presents the main performances of published data about H_2O_2 sensors based on different modified materials. It also shows competitive performance with low applied potential ($E_{app.}$ = -0.25 V) and low detection limit (1 μM) in the literature. Particularly, this hybrid composite is so active indicating a bifunctional sensor for determination of NADH and H_2O_2.

One can conclude that the active hybrid composite shows competitive performance to other materials (Table 2 & 3). It has the excellent ability to determine both NADH and H_2O_2 due to low detection limit, low working potential, and high current response, suggesting as a bifunctional sensor to determine NADH and H_2O_2 in the biosensing system.

Table 2. Performance for sensing NADH with various materials modified electrodes**.**

Modified materials	$E_{app.}$[a] (V vs. Ag/AgCl)	LOD[b] (μM)	Sensitivity (μA mM^{-1} cm^{-2})	Ref.
PNR-FAD	0.10	10	21.5	[22]
Highly ordered mesoporous carbon	0.25	1.61	93	[38]
Chemically reduced graphene oxide	0.45	10	2.68	[39]
Graphite/PMMA	0.45	3.5	68	[40]
MWCNT/poly-Xa	0.45	0.1	2.2	[41]
polyluminol/MWCNTs	0.10	0.6	183.9	[42]
ERGO-PTH/GC	0.40	0.1	143	[43]
poly-Xa/FAD/MWCNTs	0.15	171	155	[44]
PAH/SPE	0.60	0.22	125.9	[45]
PAA-PNR/MWCNTs	0.05	0.1	265.8	This work

[a] $E_{app.}$ = Applied potential.
[b] LOD = Limit of detection.

Table 3. Performance for sensing H_2O_2 with various materials modified electrodes.

Modified materials	$E_{app.}$[a] (V vs. Ag/AgCl)	LOD[b] (μM)	Sensitivity (μA mM^{-1} cm^{-2})	Ref.
PMB/FAD[c]	-0.45	0.1	1109	[21]
PNR-FAD[c]	-0.45	0.1	5.4	[22]
poly-Xa/FAD/MWCNTs[c]	-0.3	100	60	[44]
Nanostructured Prussian Blue[c]	0.05	0.001	700	[46]
Conventional (unstructured) Prussian Blue[c]	0.05	0.001	500-700	[46]
Cerium oxide nanoparticles[c]	0.2	1	15	[47]
Polymer/Pt nanoparticle[d]	0.6	0.042	500	[48]
Carbon film/nano-Pt[d]	0.6	0.0075	56	[49]
Ensembles of nano-Pt[d]	0.5	0.0005	21	[50]
PAA-PNR/MWCNT[c]	-0.25	1	10.3	This work

[a] $E_{app.}$ = Applied potential.
[b] LOD = Limit of detection.
[c] Sensing of H_2O_2 by its reduction.
[d] Sensing of H_2O_2 by its oxidation.

3.4 Interference study of the PAA-PNR/MWCNTs composite

The PAA-PNR/MWCNTs modified electrode was studied with the interference effect on amperometric determination of NADH and H_2O_2.

It was examined in the presence of several interferants including ascorbic acid, dopamine, uric acid, L-cysteine, and L-cystine ($E_{app.}$ = +0.05 V, -0.25 V). Fig. 8 shows the amperograms of PAA-PNR/MWCNTs/GCE examined for NADH with potential interferants. No much interference occurred in the amperograms. One can conclude that the modified electrode can avoid interference from most of interferants to be a good electrocatalyst to determine NADH and H_2O_2.

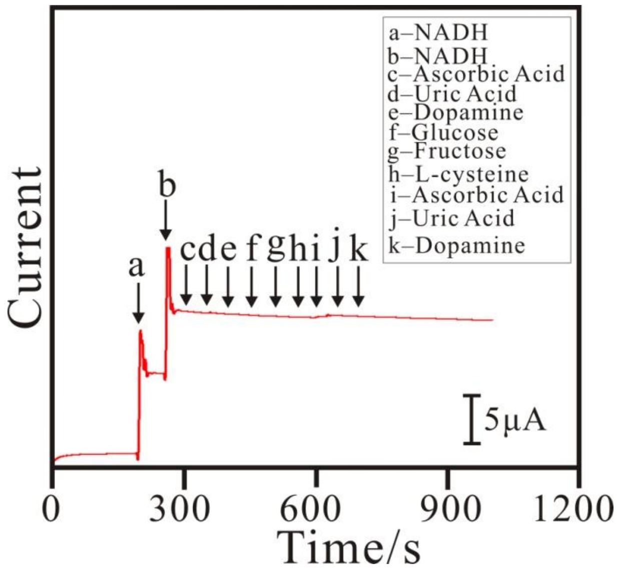

Fig. 8. Amperograms of PAA-PNR/MWCNTs/GCE examined with additions of potential interferants ($E_{app.}$ = +0.05 V): (a) 1×10^{-4} M NADH, (b) 1×10^{-4} M NADH, (c) 1×10^{-6} M ascorbic acid, (d) 1×10^{-6} M uric acid, (e) 1×10^{-6} M dopamine, (f) 1×10^{-3} M glucose, (g) 1×10^{-3} M fructose, (h) 1×10^{-3} M L-cysteine, (i) 1×10^{-4} M ascorbic acid, (j) 1×10^{-3} M uric acid, and (k) 1×10^{-3} M dopamine. Electrode rotation speed = 1000 rpm.

3.5 Stability study of the PAA-PNR/MWCNTs modified electrodes

The reproducibility and stability of the sensor were evaluated. Five PAA-PNR/MWCNTs electrodes were investigated at +0.05 V to compare their amperometric current responses. The relative standard deviation (R.S.D.) was 1.2%, indicating that the preparation method was highly reproducible. Ten successive measurements of NADH on one PAA-PNR/MWCNTs electrode yielded an R.S.D. of 2.7%, indicating that the sensor was stable. The long-term stability of the sensor was also evaluated by measuring its current response to NADH within a 7-day period. The sensor was exposed to air and its sensitivity was tested every day. The current response of PAA-PNR/MWCNTs electrode was approximately 90% of its original counterpart, which can be mainly attributed to the chemical stability of PAA and PNR on MWCNTs

4. Conclusions

PAA and PNR hybrid films can be successfully prepared on electrode surface and the coimmobilization can be further enhanced by MWCNTs. The PAA-PNR/MWCNTs electrode is electrochemically characterized and examined as a novel NADH sensor, which presents attractive analytical features such as high sensitivity, low overpotential, low detection limit, strong stability, and good reproducibility. This modified electrode also exhibits activity towards H_2O_2. As the result, the PAA-PNR/MWCNTs electrode can be a high sensitive NADH sensor and used as a bifunctional sensor to determine both NADH and H_2O_2. It approaches the prospect for effective determination of NADH and H_2O_2 due to low overpotential, low detection limit, high sensitivity, bifunction, and low cost.

Acknowledgements

This work was supported by the National Science Council of Taiwan (ROC).

Notes and references

Electroanalysis and Bioelectrochemistry Lab, Department of Chemical Engineering and Biotechnology, National Taipei University of Technology, No.1, Section 3, Chung-Hsiao East Road, Taipei 106, Taiwan (ROC). Fax: (886)-2-27025238; Tel: (886)-2-27017147; E-mail: smchen78@ms15.hinet.net

† Electronic Supplementary Information (ESI) available: [details of any supplementary information available should be included here]. See DOI: 10.1039/b000000x/

‡ Footnotes should appear here. These might include comments relevant to but not central to the matter under discussion, limited experimental and spectral data, and crystallographic data.

1 L. Gorton and E. Dominguez, Electrochemistry of NAD(P)$^+$/NAD(P)H in Encyclopedia of Electrochemistry, vol. 9, Wiley-VCH, Weinheim, 2002, pp. 67–143.
2 A. Bergel, J. Souppe and M. Comtat, *Analytical Biochemistry*, **179**, 1989, 382–388.
3 Y. Yan, W. Zheng, L. Su, L. Mao, *Advanced Materials*, 2006, **18**, 2639–2643.
4 A. Radoi and D. Compagnone, *Bioelectrochemistry*, 2009, **76**, 126–134.
5 J. Moiroux and P.J. Elving, *Analytical Chemistry*, 1978, **50**, 1056–1062.
6 Z. Samec and P.J. Elving, *Journal of Electroanalytical Chemistry*, 1983, **144**, 217–234.
7 W.J. Blaedel and R.A. Jenkins, *Analytical Chemistry*, 1975, **47**, 1337–1343.
8 M. Musameh, J. Wang, A. Merkoci and Y. Lin, *Electrochemistry Communications*, 2002, **4**, 743–746.
9 M.G. Zhang, A. Smith and W. Corski, *Analytical Chemistry*, 2004, **76**, 5045–5050.
10 C. Deng, J. Chen, X. Chen, C. Xiao, Z. Nie and S. Yao, *Electrochemistry Communications*, 2008, **10**, 907–909.
11 X. Yi, X.J. Huang and Y.C. Hong, *Analytica Chimica Acta*, 1999, **391**, 73–82.
12 S.H. Chen, R. Yuan, Y.Q. Chai, L.Y. Zhang, N. Wang and X.L. Li, *Biosensors and Bioelectronics*, 2007, **22**, 1268–1274.
13 B. Wang, J.J. Zhang, Z.Y. Pan, X.Q. Tao and H.S. Wang, *Biosensors and Bioelectronics*, 2009, **24**, 1141–1145.
14 J.L. Tang, B.Q. Wang, Z.Y. Wu, X.J. Han, S.J. Dong and E.K. Wang, *Biosensors and Bioelectronics*, 2003, **18**, 867–872.
15 Q. Xu, J.J. Zhu and X.Y. Hu, *Analytica Chimica Acta*, 2007, **597**, 151–156.
16 B.S.B. Salomi and C.K. Mitra, *Biosensors and Bioelectronics*, 2007, **22**, 1825–1829.
17 Y. Liu, J.P. Lei, H.X. Ju and Talanta, 2008, **74**, 965–970.
18 A.K. Sarma, P. Vatsyayan, P. Goswami and S.D. Minteer, *Biosensors and Bioelectronics*, 2009, **24**, 2313–2322.
19 B.D. Malhotra, A. Chaubey and S.P. Singh, *Analytica Chimica Acta*, 2006, **578**, 59–74.
20 T. Rajesh and D. Ahuja Kumar, *Sensors and Actuators B*, 2009, **136**, 275–286.
21 K.C. Lin, C.Y. Yin and S.M. Chen, *Sensors and Actuators B*, 2011, **157**, 202–210.
22 K.C. Lin and Y.C. Lin, S.M. Chen, *Analyst*, 2012, **137**, 186–194.
23 R.H. Baughman, A.A. Zakhidov and W.A.D. Heer, *Science*, 2002, **297**, 787–792.

24 P.R. Lima, W.D.J.R. Santos, A.B. Oliveira, M.O.F. Goulart and L.T. Kubota, *Biosensors and Bioelectronics*, 2008, **24**, 448–454.

25 S. Hrapovic, Y. Liu, K.B. Male and J.H.T. Luong, *Analytical Chemistry*, 2004, **76**, 1083–1088.

26 J. Sandler, M. Schaffer, T. Prasse, W. Bauhofer, K. Schulte and A.H. Windle, *Polymer*, 1999, **40**, 5967–5971.

27 C.Y. Wei, D. Srivastava and K.J. Cho, *Nano Letters*, 2002, **2**, 647–650.

28 M.G. Hughes, Z. Chen, M.S.P. Schaffer, D.J. Fray and A.H. Windle, *Chemistry of Materials*, 2002, **14**, 1610–1613.

29 K.H. An, S.Y. Jeong, H.R. Hwang and Y.H. Lee, *Advanced Materials*, 2004, **16**, 1005–1009.

30 E. Kymakis and G.A.J. Amaratunga, *Applied Physics Letters*, 2002, **80**, 112–114.

31 H.S. Woo, R. Czerw, S. Webster, D.L. Carroll, J.W. Park and J.H. Lee, *Synthetic Metals*, 2001, **116**, 369–372.

32 I. Musa, M Baxendale, G.A.J. Amaratunga and W. Eccleston, *Synthetic Metals*, 1999, **102**, 1250.

33 J.N. Coleman, S. Curran, A.B. Dalton, A.P. Davey, B. McCarthy, W. Blau and R.C. Barklie, *Synthetic Metals*, 1999, **102**, 1174–1175.

34 A.A. Karyakin, E.E. Karyakina and H.L. Schmidt, *Electroanalysis*, 1999, **11**, 149–155.

35 J. Zeng, W. Wei, X. Zhai, P. Yang, J. Yin, L. Wu, X. Liu, K. Liu and S. Gong, *Microchimica Acta*, 2006, **155**, 379–386.

36 C. Priya, G. Sivasankari and S.S. Narayanan, *Colloids and Surfaces B: Biointerfaces*, 2012, **97**, 90–96.

37 S.M. Chen and K.C. Lin, *Journal of Electroanalytical Chemistry*, 2001, **511**, 101–114.

38 M. Zhou, L. Shang, B. Li, L. Huang and S. Dong, *Electrochemistry Communications*, 2008, **10**, 859–863.

39 M. Zhou, Y. Zhai and S. Dong, *Analytical Chemistry*, 2009, **81**, 5603–5613.

40 H. Dai, H. Xu, Y. Lin, X. Wu and G. Chen, *Electrochemistry Communications*, 2009, **11**, 343–346.

41 F.D.A.D.S. Silva, C.B. Lopes, E.D.O. Costa, P.R. Lima, L.T. Kubota and M.O.F. Goulart, *Electrochemistry Communications*, 2010, **12**, 450–454.

42 K.C. Lin, C.Y. Yin and S.M. Chen, *Analyst*, 2012, **137**, 1378–1383.

43 Z. Li, Y. Huang, L. Chen, X. Qin, Z. Huang, Y. Zhou, Y. Meng, J. Li, S. Huang, Y. Liu, W. Wang, Q. Xie and S. Yao, *Sensors and Actuators B*, 2013, **181**, 280–287.

44 K.C. Lin, Y.S. Li and S.M. Chen, *Sensors and Actuators B*, 2013, **184**, 212–219.

45 L. Rotariu, O.M. Istrate and C. Bala, *Sensors and Actuators B*, 2014, **191**, 491–497.

46 A.A. Karyakin, E.A. Puganova, I.A. Bolshakov and E.E. Karyakina, *Angewandte Chemie*, 2007, **119**, 7822–7824.

47 A. Mehta, S. Patil, H. Bang, H.J. Cho and S. Seal, *Sensors and Actuators A*, 2007, **134**, 146–151.

48 P. Karam and L.I. Halaoui, *Analytical Chemistry*, 2008, **80**, 5441–5448.

49 T. You, O. Niwa, M. Tomita and S. Hirono, *Analytical Chemistry*, 2003, **75**, 2080–2085.

50 C. Sudip and R.C. Retna, *Biosensors and Bioelectronics*, 2009, **24**, 3264–3268.